

1 **Lead and slant on the geometry of coiling in gastropods**

2

3 Ido Filin *

4 * Corresponding author. E-mail: ido@filin.fi

5

6 Running headline: Geometry of coiling.

7 Supplementary material: SI appendix.

8 The author(s) declare(s) no conflict of interest.

9 This manuscript was compiled on 27 April 2026.

10 **Abstract**

11 Molluscan shells have been studied with various geometric models. Here I show that
12 *lead angle*, the defining slope of a conical helix, emerges as a more useful parameter in
13 morphometric analyses and (adaptationist) interpretation of covariation in coiling
14 parameters. The widely used apical semiangle becomes redundant and uninformative, a
15 passive consequence of taxon-specific lead angles and plasticity in growth (expansion rate).
16 Treating coiled shells as conical helices, and extending to *logarithmic slant helices* (curves of
17 precession), provides insights into ontogenetic allometry, irregular coiling, previously
18 formulated shell models, and unifying fixed- and moving-frame approaches.

19

20 **Keywords:** allometry, conchology, logarithmic spiral, ontogeny, slant helix, theoreti-
21 cal morphology,

22 Note

23 The equiangular, or logarithmic, spiral has a long and distinguished history, going back to
24 Descartes, Torricelli, Christopher Wren, Newton, Halley, and the Bernoullis (Thompson
25 [1942] 1992; Archibald 1918; Hammer 2016). Its application in biology, however, only picked
26 up with Canon (Henry) Moseley and Carl Friedrich Naumann around 1840, who applied it to
27 the study of molluscan shells, largely due to the rapid development of paleontology in the
28 19th century (Moseley 1838, 1842; Naumann 1845; Thompson [1942] 1992; Raup 1966;
29 Vinarski 2014). Much of this earlier work on modeling and measurement of shells is
30 thoroughly and eloquently summarized in D’Arcy Thompson’s *magnum opus* “On Growth
31 and Form” (Thompson [1942] 1992).

32 In “The geometry of coiling in gastropods”, Raup (1961) sketched an earlier version of his
33 parameter set for coiled geometries, that would later develop into theoretical morphology
34 and the morphospace concept (Raup & Michelson 1965; Raup 1966, 1967; McGhee 1999;
35 Gerber 2017). Essentially, though, Raup’s model is a reformulation of the original *conispiral*
36 parametrization of Moseley (1838) and Thompson ([1942] 1992) – a logarithmic spiral
37 wrapped around a cone of *apical semiangle*, β , rather than winding on a plane (planispiral
38 coiling, $\beta \rightarrow \pi/2$; Fig. 1A,D). Its defining feature is a fixed *spiral angle*, α , between the tangent
39 of the spiral and its pole (or apex of the cone; hence, equiangular; Fig. 1A).

40 Conical logspirals also arise from fixed standardized *curvature* and *torsion* in the
41 *differential geometric* formulation of Okamoto (1988), a local (moving) frame analysis
42 (Fig. 1B) that he named the ‘growing tube’ model. A third alternative parameterization views
43 the conical logspiral as a *conical helix* (Fig. 1C). The defining feature of a helix (more
44 accurately, general or generalized helix, or curve of constant slope; Nutbourne & Martin
45 1988; Scofield 1995; Rice 1998; SI) is the constant angle its tangent makes with some fixed
46 direction. This direction determines the coiling axis, and the constant slope will be measured
47 in this study by the downward angle of the coil, or helical thread, termed *lead angle*, λ in
48 Fig. 1D. (Preserving here the distinction between ‘pitch’ and ‘lead’, in the case of

49 multi-thread or -strand helical structures, i.e., double or triple helices, or multi-start screws;
50 see SI for more on terminology). If the coils wrap around a cone ($0 < \beta < \pi/2$), rather than a
51 cylinder ($\beta \rightarrow 0$; the familiar circular helices of springs and corkscrews), such a conical helix
52 is also a logarithmic conispiral. I dub this third parameterization *conihelical*.

53 In the words of D'Arcy Thompson, "It seems a complicated affair; but it is only a pathway
54 winding at a steady slope up a conical hill ... a certain ensemble, or bunch, of these spiral
55 curves in space constitutes the self-similar surface of the shell" (Thompson [1942] 1992). In
56 this note, I explore how conical helices and their "steady slope", or lead angle, have
57 underappreciated implications to morphometrics, interpretations of covariation in coiling
58 parameters, and unifying *fixed-* and *moving-frame* approaches to theoretical morphology. In
59 addition, conical helices can be extended to *slant helices*, particularly the *logarithmic slant*
60 *helix* that I present here, to gain better understanding of ontogenetic allometry, irregular
61 coiling, and previously formulated models of allometric spirals.

62 As hinted in the above quote, a shell is not a single conispiral, but a three-dimensional
63 structure made of "a bunch" of such spirals — the *multispiral* approach (Fig. 1E; also called
64 multivector; Thompson [1942] 1992; Bayer 1978; McGhee 1978, 1999; Savazzi 1990).
65 Alternatively, a shell can be described by a *generating curve*, a closed figure that sweeps
66 through space along a spiral *centerline* (Fig. 1F; Thompson [1942] 1992; Raup 1961, 1966;
67 Okamoto 1988; roughly corresponding to the 'aperture trajectory' of Stone 1995,
68 'curve-skeleton' of Monnet *et al.* 2009, 'ontogeny axis' of Liew & Schilthuizen 2016, or
69 'internal spiral' of Larsson *et al.* 2020). While called fictitious and an artificial construction
70 (Moulton *et al.* 2012; Moulton & Goriely 2012), the centerline seems a necessary evil, being a
71 central feature of most theoretical morphological and morphometric shell models (Raup
72 1966; Okamoto 1988; Liew & Schilthuizen 2016; Larsson *et al.* 2020; eventually, also Moulton
73 & Goriely 2012 use it).

74 In self-similar isometrically growing conihelical shells, the different spirals that make the
75 shell's surface, by geometric necessity, differ in spiral angle, α , apical semiangle, β , and lead
76 angle, λ (Fig. 1E). However, they all share a single common value of exponential *expansion*

77 rate, γ , with respect to revolution angle, θ (Illert 1983). Given linear measures of shell size,
 78 such as aperture size, a and b (Fig. 1F), centerline radius and height, r and z (Fig. 1D), or
 79 centerline *arclength*, s , measured from the pole (or conical apex), one can define separate
 80 expansion parameters for each. However, for self-similar conihelical shells, these expansion
 81 rates are all equal, $\gamma_s = \gamma_a = \gamma_b = \gamma_z = \gamma_r = \gamma$. Alternatively, growth and size can be measured
 82 w.r.t arclength, s , rather than revolution angle, θ . For example, the relations $a(s)$ and $b(s)$, for
 83 aperture size, introduce Ackerly's (1989a) *dilation* parameter, which I denote here by
 84 $q_a = da/ds$ and $q_b = db/ds$. In isometric conihelical shells, q_a and q_b are constants,
 85 representing the opening angles of the expanding 'trumpet' or 'cone' (Ekaratne & Crisp 1983;
 86 Ackerly 1989a; Vermeij 2002) that is coiled upon itself to make the spiral shell. Dilation
 87 factors for centerline r and z are just $q_r = \cos \alpha \sin \beta$ and $q_z = \sin \lambda = \cos \alpha \cos \beta$.

88 A set of formulas relates the conispiral, conihelical, and differential geometric
 89 parameterizations to each other and to expansion rates. One such formula is the
 90 aforementioned expression for q_z , relating lead angle, λ , to spiral angle, α . For expansion
 91 rate,

$$92 \quad \cot \alpha \sin \beta = \gamma \quad [1]$$

93 (Moseley 1842; Thompson [1942] 1992; Raup & Graus 1972; Løvtrup & von Sydow 1974;
 94 Ekaratne & Crisp 1983; Illert 1983). Gastropod shells usually exhibit several complete whorls.
 95 Consequently, expansion rate is typically small, $\gamma \leq 0.2$ (Thompson [1942] 1992; Cameron
 96 1981), leading to a similar, approximate, expression for the conihelical parameterization,

$$97 \quad \tan \lambda \tan \beta \approx \gamma \quad [2]$$

98 (the exact expression being $\tan \lambda \tan \beta = \gamma / \sqrt{1 + \gamma^2}$; see SI for discussion of approximation
 99 errors), demonstrating the three-way covariation of expansion rate, apical semiangle and
 100 lead angle.

101 Many empirical studies of shell coiling, in the past 50 years, have provided estimates of
 102 Raup's T and W parameters; or in terms of this study, $\tan \beta = 1/T$ and $\gamma = \ln W/2\pi$
 103 respectively. Covariation of $\tan \beta$ and γ may point to adaptation, such as for mechanical

104 strength, postural stability or economical shell construction (Raup 1966; Noshita *et al.* 2012;
105 Okabe & Yoshimura 2017; Páll-Gergely *et al.* 2024), and is usually interpreted through Raup's
106 (1966) condition for tight coiling, or whorl overlap, $\tan \beta > \sinh(\pi\gamma)$, given circular apertures
107 (SI). (Alternatively, $\sin \beta > \tanh(\pi\gamma)$); corresponding to the expression by Clarke *et al.* 1999,
108 accounting for the typo in their equation, and the difference in definition of apical angle; SI).
109 However, for small γ , typical of most gastropods, the whorl overlap boundary is practically
110 indistinguishable from the seemingly arbitrary condition $\lambda < \arctan(1/\pi)$ (0.318 or 17.66°;
111 Fig. 2A; SI). Similar conditions can be formulated for non-circular apertures (SI). A geometric
112 constraint on lead (or spiral) angle, combined with variation in growth rate (shell expansion),
113 can therefore produce, given Eq.[2], the empirically observed direct relation between $\tan \beta$
114 and γ .

115 Past hints to the relative constancy of lead angles can also be glimpsed from observations
116 of ontogenetic patterns, where measurements of $\tan \beta$ and γ at different whorls, or
117 developmental stages, vary together so to preserve an almost fixed ratio (e.g., Newkirk &
118 Doyle 1975; Hutchinson 1989; Clarke *et al.* 1999). In particular, Ekaratne & Crisp's (1983)
119 shell-height-to-arclength-ratio contains a $1/\sec \alpha \sec \beta$ factor, which is just $q_z = \sin \lambda$ of this
120 study. In fact, their formula can be rewritten as $H/s = z/s + b/s = q_z + q_b = \sin \lambda + q_b$ (SI).
121 Lead angle, therefore, a defining feature of conical helices, emerges as a more useful
122 parameter for interpreting morphometric (co)variation (Fig. 2B). Variation in apical
123 semiangle (β ; Fig. 2A) follows as a passive consequence of growth (variation in γ) and
124 geometry (lead angle, λ) of the expanding centerline spiral (Eq.[2]).

125 Lead angle, however, is expected to vary ontogenetically to some degree. For example,
126 Savazzi (1990) discussed deviated protoconchs (see also Frýda & Ferrová 2011); van Osselaer
127 & Grosjean (2000) fitted conispirals piecewise to several species, and showed three
128 ontogenetic phases – protoconch, and early and late conispiral phases – with different
129 coiling parameters; and Newkirk & Doyle (1975) reported values of coiling parameters for
130 embryos and adults in a study of geographic variation in the rough periwinkle, *Littorina*
131 *saxatilis* (Fig. 2).

132 Variation in lead angle can be further understood by considering the differential geometric
133 parameterization. In helices, coiling angle per unit of centerline arclength, $d\theta/ds$, is
134 measured by the norm of the *Darboux vector*, $\mathbf{u} = u\hat{\mathbf{u}}$, the rotation vector of the Frenet frame
135 along its defining space curve (Fig. 1B; Chouaieb *et al.* 2006; Goriely 2017). In generalized
136 helices, $\hat{\mathbf{u}}$ coincides with the fixed coiling axis. The norm of the Darboux vector, $\|\mathbf{u}\| = u$, is
137 the ‘compound curvature’ of Nutbourne & Martin (1988), the ‘first alternative curvature’ of
138 Güzelkardeşler & Şahiner (2024), and the familiar $\sqrt{\kappa^2 + \tau^2}$ of differential geometric literature
139 (also D_G and A_G of Noshita 2014 and Noshita *et al.* 2016, who used Okamoto’s growing tube
140 formulation; clearly related in their expressions to angular rate, $d\theta/ds$). In this note, I refer
141 to u as *local coiling*. The constant lead angle of general helices is determined by the
142 torsion-curvature ratio, $\tan \lambda = \tau/\kappa$, $\kappa = u \cos \lambda$, and $\tau = u \sin \lambda$.

143 Conical helices are further defined by local coiling that is inversely proportional to
144 arclength, s (Nutbourne & Martin 1988). We can, therefore, write $u = \tilde{u}/s$, where \tilde{u} is
145 constant dimensionless *standardized local coiling* (though the ‘standardization’ here is
146 different than Okamoto’s). Arclength expansion rate, γ_s , is then related to (standardized)
147 local coiling by the simple and intuitive relation $\gamma_s = 1/\tilde{u}$ (SI). As local coiling and curvature
148 increase, the conical helix coils tighter, and less arclength growth and radial expansion is
149 gained per full revolution. Hence, more whorls are required for a specified amount of
150 (relative) growth. This helps to explain the association of high-spined species with large
151 numbers of whorls (Cain 1980) and Gould’s so-called “jigsaw constraint”, originally observed
152 in his study of *Cerion* (Gould 1989; Béguinot 2021).

153 Allometric modifications of conical helices, such as the logarithmic *helicospiral* model,
154 derived many times in various guises (essentially, $\gamma_z \neq \gamma_r$; Kohn & Riggs 1975; Bayer 1978;
155 Cortie 1989; Schindel 1990; Savazzi 1990; Fowler *et al.* 1992; Stone 1995; Tursch 1997; van
156 Osselaer & Grosjean 2000; Urdy *et al.* 2010; Swan 2015; Larsson *et al.* 2020), and Harary &
157 Tal’s (2011)’s ‘natural 3D spiral’, do not have constant lead angles, and therefore, are not
158 generalized helices. Rate of change in lead angle, $\lambda' = d\lambda/ds$, is equivalent to the ‘second
159 alternative curvature’ of Uzunoğlu *et al.* (2016) and Güzelkardeşler & Şahiner (2024) (see SI).

160 If $\lambda' \neq 0$, the Darboux vector of local coiling and the fixed coiling axis of the helicospiral do
 161 not coincide, as the former now precesses around the latter (Fig. 1G). The precession axis is

$$162 \quad \mathbf{w} = w\hat{\mathbf{w}} = \mathbf{u} + \lambda'\hat{\mathbf{n}} = u\hat{\mathbf{u}} + \lambda'\hat{\mathbf{n}}, \quad [3]$$

$$w = \|\mathbf{w}\| = \sqrt{u^2 + (\lambda')^2} = \sqrt{\kappa^2 + \tau^2 + (\lambda')^2},$$

163 dubbed here respectively vector and rate of *global coiling*. This total coiling rate contains
 164 both a local coiling component, u , and a λ' component (first and second ‘alternative
 165 curvatures’ of [Uzunoğlu et al. 2016](#) and [Güzelkardeşler & Şahiner 2024](#); generalized helices
 166 are obtained when $\lambda' = 0$).

167 Four decades ago, [Løvtrup & Løvtrup \(1988\)](#) attempted to “move the β parameter down to
 168 the mantle edge”. In other words, derive a parameter of global shell shape from local
 169 processes occurring at the aperture. [Løvtrup & Løvtrup](#)’s partial solution was to replace β
 170 with the ratio of maximum and minimum growth rates around the aperture. An explanation
 171 that [Hutchinson \(1990\)](#) debunked shortly after. Through Eqs.[1] and [2], however, the apical
 172 semiangle can indeed be “eliminated”, or “moved down” to the aperture, as γ , α , and λ are
 173 defined at the growing tip (i.e., tangent) of conispirals, or conihelices. The distinction
 174 between fixed- (conispiral and conihelical) and moving-frame (differential geometric)
 175 parameterizations, thus, begins to blur.

176 Another defining feature of fixed-frame models is, for obvious reasons, the fixed coiling
 177 axis. Rate of change in the direction of local coiling, $\hat{\mathbf{u}}$, is given by $\hat{\mathbf{u}}' = \mathbf{w} \times \hat{\mathbf{u}} =$
 178 $u\hat{\mathbf{u}} \times \hat{\mathbf{u}} + \lambda'\hat{\mathbf{n}} \times \hat{\mathbf{u}} = \lambda'\hat{\mathbf{n}} \times \hat{\mathbf{u}}$. In conihelical shells $\lambda' = 0$, and the Darboux vector, \mathbf{u} , defines
 179 the fixed coiling axis. Thus, given starting coiling direction (initial condition), conispiral
 180 coiling can be defined by apical and spiral angles, by lead angle and expansion rate, by lead
 181 angle and standardized local coiling, \tilde{u} , or by [Okamoto](#)’s standardized curvature and torsion
 182 (SI). In all four cases, if parameter values remain fixed, the initial coiling direction is
 183 maintained ($\hat{\mathbf{u}}' = 0$), becoming a fixed axis, and self-similar conispiral shells result. That is
 184 another metric by which the distinction between fixed- and moving-frame parametrizations
 185 seems superfluous.

186 Irregular coiling, allometry, or other deviations from self-similar conihelical geometry,

187 always require a change in parameter values (notably, lead angle). Gradual rotation of the
 188 local coiling axis, $\hat{\mathbf{u}}$, thus, occurs simultaneously with (transient) change in lead angle
 189 ($\lambda' \neq 0$), and by precessing around the vector of global coiling, \mathbf{w} (Fig. 1G). That is, in fact,
 190 another direct consequence of conihelical geometry; this time, prescribing a testable
 191 hypothesis on how shell geometry can deviate from isometric conihelical. Some evidence in
 192 support of this hypothesis appears in Ackerly's (1989b) visual and stereographical analyses
 193 of *Vermicularia*, which possesses a tightly coiled conspiral juvenile phase, followed by an
 194 open-coiled geometry that differs in both coiling axis and lead angle. Similarly, his analysis
 195 of *Distorsio* shows that lead angle varies among consecutive episodic growth increments,
 196 while the coiling axis precesses with an angular radius of roughly four to seven degrees.
 197 Savazzi (1996) provides examples from several species of *Tenagodus* (syn. *Siliquaria*) and
 198 *Vermicularia* that follow the same rule of simultaneous change in coiling axis and in lead
 199 angle. Particularly extreme cases occur in microsnails (Clements *et al.* 2008; Liew *et al.* 2014)
 200 and in irregularly coiled (heteromorph) ammonoids (Okamoto 1988, 1996).

201 Initially, the allometric logarithmic helicospiral ($\gamma_z \neq \gamma_r$) seems to contradict the
 202 hypothesis, as lead angle increases ($\gamma_z > \gamma_r$) or decreases ($\gamma_z < \gamma_r$), while the coiling axis
 203 remains fixed. Similarly, in Harary & Tal's (2011)'s 'natural 3D spiral', lead angle varies
 204 smoothly between a starting value, λ_0 , and an asymptotic value, λ_∞ , at large arclengths;
 205 essentially, converging to a conspiral (though adult size and shape may be obtained well
 206 before that asymptote is reached). However, when the direction of $\mathbf{w} = u\hat{\mathbf{u}} + \lambda'\hat{\mathbf{n}}$ does not
 207 change, it acts as the new fixed coiling axis of the shell; its magnitude, $w = \sqrt{u^2 + (\lambda')^2}$, is the
 208 coiling rate around that axis (i.e., revolution angle per unit growth of centerline arclength,
 209 $d\theta/ds = w = \|\mathbf{w}\|$). This precession of the local moving Frenet frame around a potentially
 210 fixed axis, $\hat{\mathbf{w}}$, is another reason why fixed- and moving-frame models should be considered in
 211 tandem, as complementary points of view.

212 The condition of fixed $\hat{\mathbf{w}}$ is satisfied, for example, when local coiling and change in lead
 213 angle are both constant, $u = \text{const}$, $\lambda' = \text{const}$. These are the 'modulated curves' of
 214 Nutbourne & Martin (1988), better known as 'curves of constant precession' (Scofield 1995).

215 Another class of curves, in which $\hat{\mathbf{w}}$ is fixed, are the already familiar conical and generalized
 216 helices. This is just the degenerate case of $\mathbf{w} = \mathbf{u}$ and $\lambda' = 0$, where the precession vanishes.
 217 Extrapolating from both curves of constant precession and curves of constant slope
 218 (generalized helices), one obtains a class of curves called *slant helices* that includes the
 219 former two as special cases. A necessary and sufficient condition for a slant helix, in the
 220 notation of this study, is $\lambda' \propto u$, or $\lambda' = \sigma u$ where $\sigma = \text{const}$ (Izumiya & Takeuchi 2004 ; SI).

221 We can proceed still one step further, and define the *logarithmic slant helix*, $u, \lambda' \propto 1/s$, or
 222 $u = \tilde{u}/s$ and $\lambda' = \sigma \tilde{u}/s$, where σ and \tilde{u} are constants (SI). While the logarithmic slant helix
 223 describes an allometrically growing shell, it does share some properties with the isometric
 224 conical helix. For example, revolution angle and arclength are similarly related through
 225 $\theta \propto \ln(s/s_0)$, and therefore arclength expands exponentially, $s = s_0 e^{\gamma_s \theta}$, where $\gamma_s = 1/\tilde{w}$,
 226 $\tilde{w} = \tilde{u}\sqrt{1 + \sigma^2}$. However, radial expansion is no longer exponential. As lead angle changes,
 227 the radial expansion rate is instantaneously given by $\gamma_r \approx \gamma_s(1 - \sigma \tilde{u} \tan \lambda)$ (SI). Centerline
 228 radius, thus, grows with negative allometry, relative to arclength ($\gamma/\gamma_s < 1$, assuming $\sigma > 0$).
 229 Yet another feature of logarithmic slant helices is that lead angle grows linearly with θ .
 230 Consecutive whorls, separated by a full revolution around the coiling axis ($\Delta\theta = 2\pi$), are
 231 always tilted relative to each other by the same amount, $\Delta\lambda = 2\pi\lambda'/w = 2\pi\sigma/\sqrt{1 + \sigma^2}$
 232 (Fig. 1H).

233 The logarithmic slant helix, thus, is a natural allometric extension of the isometric conical
 234 helix, in the sense that, instead of being fixed on the same initial value (λ_0) throughout
 235 ontogeny, lead angle grows linearly (i.e., $\lambda(\theta) = \lambda_0 + c\theta$; $c = \text{const}$). In that respect, it is the
 236 simplest case of centerline allometry, and provides insight into the more complex variation in
 237 other models (helicospirals, $\gamma_z \neq \gamma_r$, or Harary & Tal 2011). Clearly, lead angle cannot grow
 238 indefinitely, unless coiling becomes open and irregular. But, in any case, real shells have a
 239 finite number of whorls, and therefore, the logarithmic slant helix, like its older cousin, the
 240 conical helix, is a useful approximation. In particular, given expressions for centerline height
 241 and radius, $z(\theta)$ and $r(\theta)$ (SI), one can simulate such shells graphically (Fig. 1H,I).

242 **Supplementary information**

243 Additional derivations, explanations, methods, and discussion are in the supplementary
244 information document.

245 **DATA AND SOFTWARE AVAILABILITY.** All data and code are available at

246 <https://doi.org/10.5281/zenodo.19763621>, for the data analyses (Fig. 2), and at

247 <https://doi.org/10.5281/zenodo.19762139>, for the WebGL application of theoretical
248 morphology of coiled shells (Fig. 1).

249 **References**

- 250 Ackerly SC (1989a). Kinematics of accretionary shell growth, with examples from
251 brachiopods and molluscs. *Paleobiology* 15: 147–164. [10.1017/s0094837300009337](https://doi.org/10.1017/s0094837300009337).
- 252 Ackerly SC (1989b). Shell coiling in gastropods; analysis by stereographic projection.
253 *PALAIOS* 4: 374–378. [10.2307/3514561](https://doi.org/10.2307/3514561).
- 254 Araki A, Noshita K (2023). Theoretical morphological analysis of differential morphospace
255 occupation patterns for terrestrial and aquatic gastropods. *Evolution* 77: 1864–1873.
256 <https://doi.org/10.1093/evolut/qpad110>.
- 257 Archibald RC (1918). The logarithmic spiral (undergraduate mathematics clubs, topics for
258 club programs). *American Mathematical Monthly* 25: 189–193.
- 259 Bayer U (1978). Morphogenetic programs, instabilities, and evolution — a theoretical study.
260 *Neues Jahrb Geol Paläont Abh* 156: 226–261.
- 261 Béguinot J (2021). Adult shell-size regulation in conspirally-coiled shells: evidence for a
262 widespread negative covariance between whorls growth-rate and the final number of
263 whorls in land snails. *Annual Research & Review in Biology* 36: 95–106.
264 <https://doi.org/10.9734/arrb/2021/v36i1030439>.
- 265 Cain AJ (1980). Whorl number, shape, and size of shell in some pulmonate faunas. *J Conchol*
266 30: 209–221.
- 267 Cameron RAD (1981). Functional aspects of shell geometry in some british land snails. *Biol J*

268 *Linn Soc* 16: 157–167. <https://doi.org/10.1111/j.1095-8312.1981.tb01648.x>.

269 Chouaieb N, Goriely A, Maddocks JH (2006). Helices. *Proc Natl Acad Sci USA* 103: 9398–9403.

270 <https://doi.org/10.1073/pnas.0508370103>.

271 Clarke RK, Grahame J, Mill PJ (1999). Variation and constraint in the shells of two sibling
272 species of intertidal rough periwinkles (gastropoda: *Littorina* spp.). *J Zool* 247: 145–154.

273 [10.1111/j.1469-7998.1999.tb00978.x](https://doi.org/10.1111/j.1469-7998.1999.tb00978.x).

274 Clements R, Liew TS, Vermeulen JJ, Schilthuizen M (2008). Further twists in gastropod shell
275 evolution. *Biology Letters* 4: 179 – 182. <https://doi.org/10.1098/rsbl.2007.0602>.

276 Cortie M (1989). Models for mollusc shell shape. *South African Journal of Science* 85: 454–460.

277 Ekaratne SUK, Crisp DJ (1983). A geometric analysis of growth in gastropod shells, with
278 particular reference to turbinate forms. *Journal of Marine Biology Association UK* 63:
279 777–797.

280 Fowler DR, Meinhardt H, Prusinkiewicz P (1992). Modeling seashells. *Proceedings of the 19th*
281 *annual conference on Computer graphics and interactive techniques*, pp. 379–387.

282 [10.1145/133994.134096](https://doi.org/10.1145/133994.134096).

283 Frýda J, Ferrová L (2011). The oldest evidence of non-coaxial shell heterostrophy in the class
284 Gastropoda. *Bull Geosci* 86: 765–776. [10.3140/bull.geosci.1302](https://doi.org/10.3140/bull.geosci.1302).

285 Gerber S (2017). The geometry of morphospaces: lessons from the classic Raup shell coiling
286 model. *Biol Rev* 92: 1142–1155. <https://doi.org/10.1111/brv.12276>.

287 Goriely A (2017). *The Mathematics and Mechanics of Biological Growth*. Springer.

288 <https://doi.org/10.1007/978-0-387-87710-5>.

289 Gould SJ (1989). A developmental constraint in *Cerion*, with comments on the definition and
290 interpretation of constraint in evolution. *Evolution* 43: 516–539.

291 Güzelkardeşler G, Şahiner B (2024). An alternative approach to find the position vector of a
292 general helix. *Celal Bayar University Journal of Science* 20: 54–60.

293 [10.18466/cbayarfbe.1479066](https://doi.org/10.18466/cbayarfbe.1479066).

294 Hammer Ø (2016). *Perfect Shape: Spiral Stories*. Springer.

- 295 Harary G, Tal A (2011). The natural 3d spiral. *Computer Graphics Forum* 30: 237–246.
296 <https://doi.org/10.1111/j.1467-8659.2011.01855.x>.
- 297 Hutchinson JMC (1989). Control of gastropod shell shape: the role of the preceding whorl. *J*
298 *Theor Biol* 140: 431–444.
- 299 Hutchinson JMC (1990). Control of gastropod shell form via aperture growth rates. *J*
300 *Morphol* 206: 259–264.
- 301 Illert C (1983). The mathematics of gnomonic seashells. *Math Biosci* 63: 21–56.
- 302 Izumiya S, Takeuchi N (2004). New special curves and developable surfaces. *Turkish Journal*
303 *of Mathematics* 28: 153–164.
- 304 Kohn AJ, Riggs AC (1975). Morphometry of the *Conus* shell. *Syst Zool* 24: 346–359.
- 305 Larsson J, Westram AM, Bengmark S, Lundh T, Butlin RK, Butlin RK (2020). A
306 developmentally descriptive method for quantifying shape in gastropod shells. *J R Soc*
307 *Interface* 17. <http://dx.doi.org/10.1098/rsif.2019.0721>.
- 308 Liew TS, Kok ACM, Schilthuizen M, Urdy S (2014). On growth and form of irregular
309 coiled-shell of a terrestrial snail: *Plectostoma concinnum* (Fulton, 1901) (Mollusca:
310 Caenogastropoda: Diplommatinidae). *PeerJ* 2: e383.
311 <https://doi.org/10.7717/peerj.383>.
- 312 Liew TS, Schilthuizen M (2016). A method for quantifying, visualising, and analysing
313 gastropod shell form. *PLOS ONE* 11: 1–24.
314 <https://doi.org/10.1371/journal.pone.0157069>.
- 315 Løvtrup S, Løvtrup M (1988). The morphogenesis of molluscan shells: a mathematical
316 account using biological parameters. *J Morphol* 197: 53–62.
- 317 Løvtrup S, von Sydow B (1974). D'arcy Thompson's theorem and the shape of the molluscan
318 shell. *Bull Math Biol* 36: 567–575.
- 319 McGhee GR (1978). Analysis of the shell torsion phenomenon in the Bivalvia. *Lethaia* 11:
320 315–329. <https://doi.org/10.1111/j.1502-3931.1978.tb01889.x>.
- 321 McGhee GR (1999). *Theoretical Morphology: The Concept and Its Applications*. Perspectives in

- 322 Earth History and Paleobiology. Columbia University Press, New York.
- 323 Monnet C, Zollikofer C, Bucher H, Goudemand N (2009). Three-dimensional morphometric
324 ontogeny of mollusc shells by micro-computed tomography and geometric analysis.
325 *Palaeontol Electron* 12: 1–13. <https://doi.org/10.5167/uzh-23587>.
- 326 Moseley H (1838). On the geometrical forms of turbinated and discoid shells. *Philosophical
327 Transactions of the Royal Society of London* 1838: 351–370.
- 328 Moseley H (1842). On conchylometry. *Lond Edinb Dubl Phil Mag* 21: 300–305.
- 329 Moulton D, Goriely A, Chirat R (2012). Mechanical growth and morphogenesis of seashells. *J
330 Theor Biol* 311: 69–79. <https://doi.org/10.1016/j.jtbi.2012.07.009>.
- 331 Moulton DE, Goriely A (2012). Surface growth kinematics via local curve evolution. *J of
332 Math Biol* 68: 81–108.
- 333 Naumann CF (1845). Über die wahre Spirale der Ammoniten. *Annalen der Physik* 140:
334 538–543. <https://doi.org/10.1002/andp.18451400406>.
- 335 Newkirk GF, Doyle RW (1975). Genetic analysis of shell-shape variation in *Littorina saxatilis*
336 on an environmental cline. *Mar Biol* 30: 227–237. [10.1007/BF00390745](https://doi.org/10.1007/BF00390745).
- 337 Noshita K (2014). Quantification and geometric analysis of coiling patterns in gastropod
338 shells based on 3d and 2d image data. *J Theor Biol* 363: 93–104.
- 339 Noshita K, Asami T, Ubukata T (2012). Functional constraints on coiling geometry and
340 aperture inclination in gastropods. *Paleobiology* 38: 322–334. [10.1666/10060.1](https://doi.org/10.1666/10060.1).
- 341 Noshita K, Shimizu K, Sasaki T (2016). Geometric analysis and estimation of the growth rate
342 gradient on gastropod shells. *J Theor Biol* 389: 11–19.
343 <https://api.semanticscholar.org/CorpusID:39448122>.
- 344 Nutbourne AW, Martin RR (1988). *Differential geometry applied to curve and surface design*.
345 Ellis Horwood, Chichester, England.
- 346 Okabe T, Yoshimura J (2017). Optimal designs of mollusk shells from bivalves to snails.
347 *Scientific Reports* 7: 42445. <https://doi.org/10.1038/srep42445>.
- 348 Okamoto T (1988). Analysis of heteromorph ammonoids by differential geometry.

349 *Paleobiology* 31: 35–52.

350 Okamoto T (1996). Theoretical modeling of ammonoid morphology. In *Ammonoid*
351 *Paleobiology* (edited by Landman NH, Tanabe K, Davis RA), pp. 225–251. Springer US,
352 Boston, MA. https://doi.org/10.1007/978-1-4757-9153-2_8.

353 Páll-Gergely B, Sipos AÁ, Harzhauser M, Örstan A, Winkler V, Neubauer TA (2024). Many
354 roads to success: alternative routes to building an economic shell in land snails. *Evolution*
355 78: 778–786. <https://doi.org/10.1093/evolut/qpae018>.

356 Raup DM (1961). The geometry of coiling in gastropods. *Proc Natl Acad Sci USA* 47: 602–609.
357 <https://doi.org/10.1073/pnas.47.4.602>.

358 Raup DM (1966). Geometric analysis of shell coiling: general problems. *J Paleontol* 40:
359 1178–1190.

360 Raup DM (1967). Geometric analysis of shell coiling: coiling in ammonoids. *J Paleontol* 41:
361 43–65.

362 Raup DM, Graus RR (1972). General equations for volume and surface area of a
363 logarithmically coiled shell. *Mathematical Geology* 4: 307–316.

364 Raup DM, Michelson A (1965). Theoretical morphology of the coiled shell. *Science* 147:
365 1294–1295.

366 Rice SH (1998). The bio-geometry of mollusc shells. *Paleobiology* 24: 133–149.

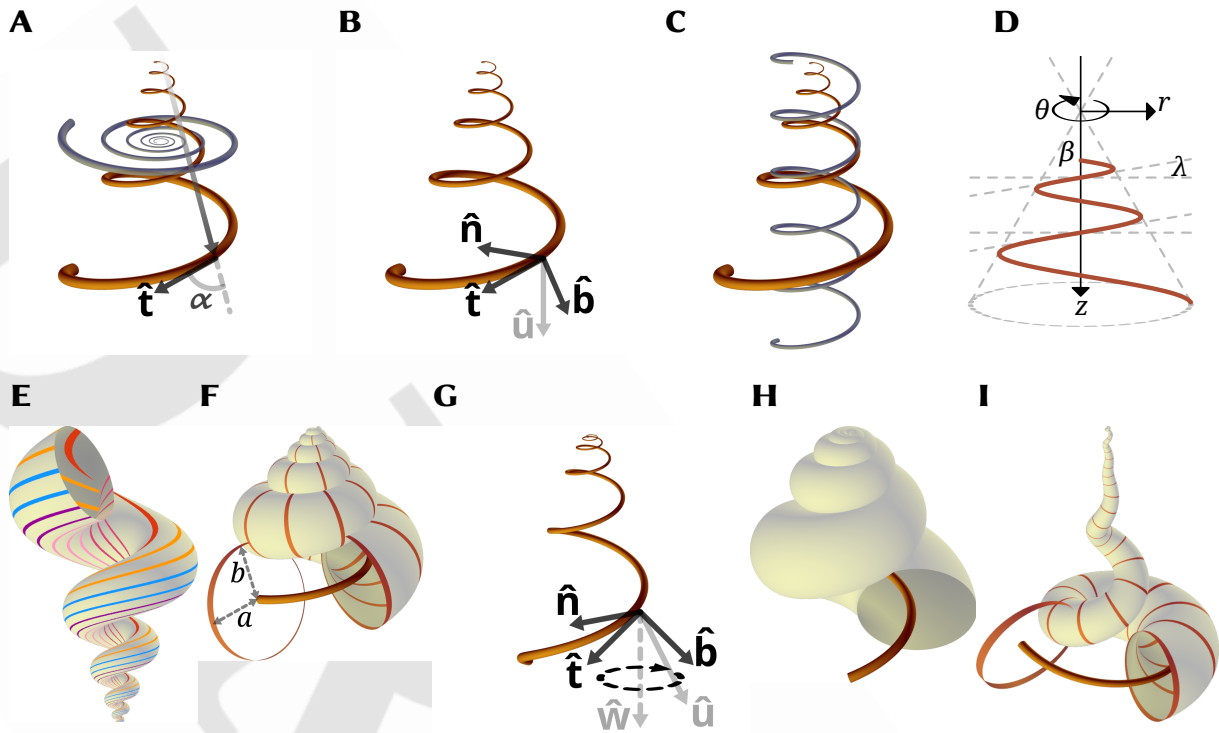
367 Savazzi E (1990). Biological aspects of theoretical shell morphology. *Lethaia* 23: 195–212.

368 Savazzi E (1996). Adaptations of vermetid and silicuarid gastropods. *Palaeontology* 39:
369 157–177.

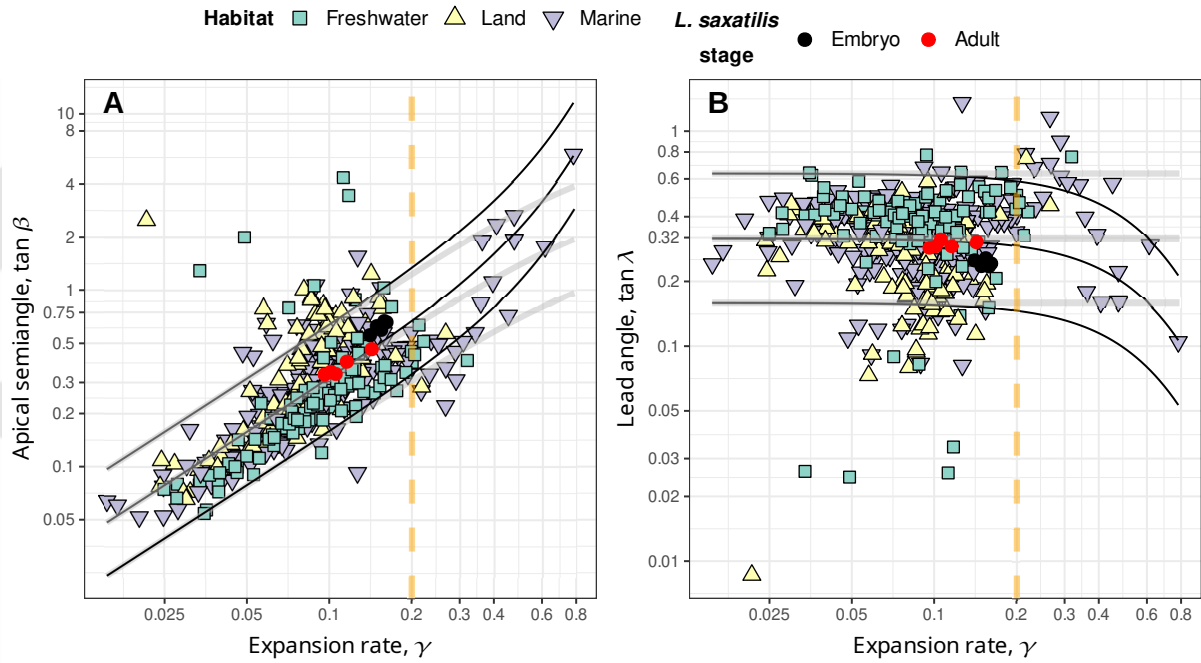
370 Schindel DE (1990). Unoccupied morphospace and the coiled geometry of gastropods:
371 architectural constraint or geometric covariation? In *Causes of Evolution: a paleontological*
372 *perspective* (edited by Ross R, Allmon W), pp. 270–304. University of Chicago Press,
373 Chicago.

374 Scofield PD (1995). Curves of constant precession. *The American Mathematical Monthly* 102:
375 531–537. <https://doi.org/10.1080/00029890.1995.12004613>.

- 376 Stone JR (1995). CerioShell: a computer program designed to simulate variation in shell form.
377 *Paleobiology* 21: 509–519.
- 378 Swan ARH (2015). Heterochrony in helicoid spiral cones: a computer model for
379 demonstrating heterochronic evolution. *Palaeontol Electron* 18: 1–11. [10.26879/510](https://doi.org/10.26879/510).
- 380 Thompson DW ([1942] 1992). *On Growth and Form: The Complete Revised Edition*. Dover,
381 New York.
- 382 Tursch B (1997). Spiral growth: The ‘Museum of all shells’ revisited. *J Molluscan Stud* 63:
383 547–554. <https://doi.org/10.1093/mollus/63.4.547>.
- 384 Urdy S, Goudemand N, Bucher H, Chirat R (2010). Allometries and the morphogenesis of the
385 molluscan shell: a quantitative and theoretical model. *J Exp Zool* 314B: 280–302.
386 [10.1002/jez.b.21337](https://doi.org/10.1002/jez.b.21337).
- 387 Uzunoğlu B, İsmail Gök, Yaylı Y (2016). A new approach on curves of constant precession.
388 *Applied Mathematics and Computation* 275: 317–323.
389 <https://doi.org/10.1016/j.amc.2015.11.083>.
- 390 van Osselaer C, Grosjean P (2000). Suture and location of the coiling axis in gastropod shells.
391 *Paleobiology* 26: 238–257.
392 [https://doi.org/10.1666/0094-8373\(2000\)026<0238:SAL0TC>2.0.CO;2](https://doi.org/10.1666/0094-8373(2000)026<0238:SAL0TC>2.0.CO;2).
- 393 Vermeij GJ (2002). Characters in context: molluscan shells and the forces that mold them.
394 *Paleobiology* 28: 41–54.
- 395 Vinarski MV (2014). The birth of malacology. when and how? *Zoosystematics and Evolution*
396 90: 1–5.



397 **Figure 1** : Theoretical morphology in a snailshell. **(A,B,C)** Three parameterizations of conical logspirals; re-
 398 spectively conispiral, differential geometric, and conihelical. **(A)** Constant spiral angle, α , between instantaneous
 399 tangent vector, $\hat{\mathbf{t}}$, and radius-vector from pole (apex) defines the conispiral parameterization. Also illustrated is
 400 the corresponding base planispiral – the projection of the conispiral onto (r, θ) -plane, perpendicular to coiling
 401 axis **(SI)**. For logarithmic conispirals, base spiral is also logarithmic, with same expansion rate, γ . **(B)** The differen-
 402 tial geometric parameterization follows the evolution of the Frenet moving frame, defined by tangent $\hat{\mathbf{t}}$, principal
 403 normal, $\hat{\mathbf{n}}$, and binormal $\hat{\mathbf{b}} = \hat{\mathbf{t}} \times \hat{\mathbf{n}}$. The frame's rotation is defined by the Darboux vector $\mathbf{u} = u\hat{\mathbf{u}} = \tau\hat{\mathbf{t}} + \kappa\hat{\mathbf{b}} =$
 404 $u \sin \lambda \hat{\mathbf{t}} + u \cos \lambda \hat{\mathbf{b}}$; κ is curvature, and τ torsion **(SI)**. **(C)** In the conihelical parameterization, a conical logspiral is
 405 viewed as a helix with expanding radius – a conical helix. For comparison, a circular helix with same slope (i.e.,
 406 lead angle) is also illustrated. **(D)** Conical helix in side view. Api cal semiangle, β , lead angle, λ , and the cylindrical
 407 coordinate system illustrated. The z -direction coincides with the coiling axis. **(E)** Multispiral approach to shell
 408 modeling, where shell surface is defined by many spiral paths, differing in lead angle. For illustration purposes,
 409 an exaggerated open-coiled shell is shown, where slopes of inner spirals are clearly steeper. Nevertheless, all
 410 spirals share the same expansion rate, γ . **(F)** Generating curve approach to shell modeling. Shell surface defined
 411 by a closed figure (here a circle) that sweeps along a conihelical centerline. Also illustrated are the size measures,
 412 a and b (not to be confused with the binormal vector, $\hat{\mathbf{b}}$), roughly corresponding to aperture size perpendicu-
 413 lar and parallel, respectively, to the coiling axis. **(G)** In allometric shells, where centerline's lead angle varies,
 414 the Darboux vector is no longer fixed, but precesses around an axis $\mathbf{w} = w\hat{\mathbf{w}}$ that contains a λ' component **(SI)**.
 415 **(H,I)** Allometric and irregularly coiled shells with logarithmic slant helix centerline. Lead angles are initially 0
 416 (i.e., planispiral coiling), but subsequently grow at different rates. Parameters values to simulate all shell images
 417 in this figure in the WebGL application are provided in **SI**.



419 Figure 2 : Apical semiangle, as $\tan\beta$ (panel A), and lead angle, as $\tan\lambda$ (panel B), against expansion rate,
 420 $\gamma = \ln W/2\pi$, from the data in Noshita *et al.* (2012) and Araki & Noshita (2023) on coiling parameters of over
 421 400 species freshwater, marine, and terrestrial gastropods, and the data of Newkirk & Doyle (1975) on em-
 422 bryos and adults of *Littorina saxatilis* from five different populations in Nova Scotia. In both panels, a vertical
 423 dashed line for $\gamma = 0.2$ marks roughly the domain of validity for small- γ approximations (SI), where neverthe-
 424 less most data lies. Illustrated curves, however, were drawn using full (exact, non-approximate) expressions (SI).
 425 (A) When apical semiangle is plotted against expansion rate, a clear linear trend is visible. Solid black lines
 426 indicate boundaries for whorl-overlap, $\tan\beta > (1/\rho) \sinh(\pi\gamma)$, for $\rho = 0.5, 1, 2$ (upper to lower; where ρ is de-
 427 fined as $\rho = b/a$, ratio of the aperture sizes; $\rho = 1$ means a circular aperture) that separates tightly-coiled (above
 428 boundary line) and open-coiled shells (below boundary line). In the range $\gamma < 0.2$, such boundary curves for
 429 tight-coiling, however, are practically indistinguishable from relationships that fixed lead angles in Eq.[2] pre-
 430 scribe ($\tan\beta = (\gamma/\sqrt{1+\gamma^2}) \cot\lambda$; gray lines), given $\tan\lambda = \rho/\pi$ (SI; $D = 0$ for illustrated curves; i.e., apertures
 431 touching the coiling axis). Raw values for apical angles were transformed to correspond to centerlines by dou-
 432 bling reported values of T . (B) Estimates of lead angle, $\tan\lambda$, obtained from eqn:conihelical. Compared to panel
 433 A, there is clearly less in lead angle, than in apical angle, and the linear trend disappears; suggesting independent
 434 variation in expansion rate, γ , and lead angle, λ . Black and gray solid curves correspond to those those in panel
 435 A, but in reverse order ($\rho = 2, 1, 0.5$, upper to lower respectively).

418

436

S1 **Supplementary information for “Lead and slant on the geometry of**
S2 **coiling in gastropods”**

S3

S4 Ido Filin *

S5 * Corresponding author. E-mail: ido@filin.fi

S6

S7 **Contents**

S8	S1 A note on terminology and notation	2
S9	S2 Expressions for logarithmic conispirals	3
S10	S3 Whorl-overlap condition for non-circular and displaced generating curves	4
S11	S4 Approximation errors	6
S12	S5 Differential geometric parameterization	7
S13	S6 Logarithmic slant helix	9
S14	S7 Web application	10
S15	S8 Supplementary references	10

S16 **S1 A note on terminology and notation**

S17 [Thompson \(\[1942\] 1992\)](#) defined three angles, related to the modeling of equiangular (i.e.,
S18 logarithmic) spiral shells. The spiral angle, α , is the angle between the radius-vector from the
S19 pole (or apex of the conical envelope) and the tangent to the spiral. His β denotes the apical
S20 semiangle, as in this study. His γ refers to the “angle of retardation”, relevant when
S21 considering the inner and outer margins of planispiral shells. Given that the angle of
S22 retardation has been rarely utilized since, I reclaim the symbol γ for denoting the
S23 exponential expansion rate in this study.

S24 Generalized or general helices ([Nutbourne & Martin 1988](#)) are defined by the constant
S25 slope, relative to a fixed direction. Hence the alternative term, curve of constant slope
S26 ([Scofield 1995](#)). Somewhat confusingly they are also often called ‘cylindrical helices’ ([O’Neill](#)
S27 [2006](#)), referring to a generalized cylinder. But I avoid this term here.

S28 While ‘pitch’ is used often with circular helices to refer to the slope of the helix (e.g.,
S29 [Chouaieb et al. 2006](#)), strictly speaking, pitch is the distance between adjacent threads or
S30 strands. Lead, on the other hand, is the axial progression per one full revolution of the helical
S31 structure, which is the quantity of interest in this study. Lead and pitch are the same for
S32 single-thread helices, but not for double or triple helices, such as in double- and multi-start
S33 screws and various helical structures in biology.

S34 The slope of the helix, $\tan \lambda$, can be measured by the lead angle, as in this study, by the
S35 ‘helix slope’ itself (e.g., [De Renzi & Mayoral 2024](#); also ‘rise’, [Hauser et al. 2017](#)), or by the
S36 ‘helix angle’, relative to the fixed axis (the complementary angle to the lead angle; [Nutbourne](#)
S37 [& Martin 1988](#)). The latter was referred to as ‘inclination angle’ by [Moseley \(1842\)](#), in his
S38 work on conchylometry. However, more recently, inclination angle is used to describe the
S39 orientation of the aperture itself relative to the coiling axis ([Schindel 1990](#); [Vermeij 1993](#);
S40 [Noshita et al. 2012](#)), so I avoid this term here.

S41 Finally, the quantity $u = \sqrt{\kappa^2 + \tau^2}$, which is the norm of the Darboux vector, where κ is
S42 curvature and τ is torsion, does not have a standard name. [Nutbourne & Martin \(1988\)](#) refer

S43 to it as ‘compound curvature’, and Güzelkardeşler & Şahiner (2024) call it ‘first alternative
S44 curvatrue’. Other appropriate terms may be ‘winding’ or ‘twist’, in reference to circular
S45 helices (Chouaieb *et al.* 2006; Goriely 2017). But those usually involve additional meaning in
S46 terms of mechanical properties. It is also sometimes called angular rate, speed, or velocity,
S47 though time is only implicit here, and u measures rotation angle per unit arclength, not time.
S48 In this study, I refer to the Darboux vector and its norm, as well as to \mathbf{w} and w , simply as
S49 vectors and rates of coiling, as in the end, they describe direction and rate of rotation. While
S50 the greek letter ω is often used to denote the Darboux vector and $\sqrt{\kappa^2 + \tau^2}$ (Nutbourne &
S51 Martin 1988), I avoid this notation, so not to confuse with true angular velocity in mechanics.

S52 **S2 Expressions for logarithmic conispirals**

S53 Eq.[1] of the main text, $\cot \alpha \sin \beta = \gamma$, has been derived and used enough times, so not to
S54 require any explanation (Moseley 1842; Thompson [1942] 1992; Raup & Graus 1972; Løvtrup
S55 & von Sydow 1974; Ekaratne & Crisp 1983; Illert 1983). From geometry of cones, it is easy to
S56 see that

$$S57 \quad \sin \lambda = \cos \alpha \cos \beta \quad [S1]$$

S58 (Moseley 1842; up to differences in notation and definition of lead angle), the expression for
S59 spiral height dilation, q_z . These two equations can be combined to produce

$$S60 \quad \tan \lambda \tan \beta = \frac{\gamma}{\sqrt{1 + \gamma^2}}. \quad [S2]$$

S61 Values of γ for gastropods are typically below 0.2 (Thompson [1942] 1992; Cameron 1981;
S62 Fig. 3), corresponding to relatively slower expansion and shells that exhibit several complete
S63 whorls. For small values of γ , Eq.[S2] is approximated by Eq.[2] of the main text.

S64 The *base spiral* is the projection of the spiral space curve onto the (r, θ) -plane, i.e.,
S65 perpendicular to the coiling axis. For a logarithmic conispiral, the base spiral is also
S66 logarithmic, with the same expansion rate γ . The arclength of the projection spiral is, in

S67 general, given by $\ell(\theta)$ or $\ell(s)$, and obtained by integrating $d\ell = ds \cos \lambda =$

S68 $d\theta \sqrt{r^2 + (dr/d\theta)^2}$. For conical logspirals these integrate to $\ell(s) = s \cos \lambda$ and $\ell(\theta) =$

$$S69 \quad \frac{1+\gamma^2}{\gamma} r(\theta) = \frac{1+\gamma^2}{\gamma} r_0 e^{\gamma\theta}.$$

S70 More generally, for small radial expansion rates, $\gamma_r = \gamma_r(\theta) \equiv d \ln r / d\theta \leq 0.2$, we can
 S71 observe that $d\ell = d\theta \sqrt{r^2 + (dr/d\theta)^2} = r d\theta \sqrt{1 + \gamma_r^2} \approx r d\theta$, or

$$S72 \quad \frac{d\ell}{d\theta} = r(1 + \mathcal{O}(\gamma_r^2)). \quad [S3]$$

S73 Consequently, as a first approximation we can estimate the radius of the space curve as
 S74 $r \approx d\ell/d\theta$, as long as $r(\theta)$ grows relatively slowly, $d \ln r / d\theta$ is small. Alternatively, $d\ell/d\theta$
 S75 provides an upper bound to the radius, $r(\theta)$. This approximation is used below, in relation to
 S76 the position vector of logarithmic slant helices.

S77 Finally, the expression for a conispiral shell's height-to-arclength ratio, derived by
 S78 [Ekaratne & Crisp \(1983\)](#), can be written as $(z + b)/s$ in this study, which translates to
 S79 $q_z + q_b = \sin \lambda + q_b$. Alternatively, using the steps of their derivation and following the
 S80 suture spiral on the outer surface of the shell, rather than the centerline spiral,
 S81 $(z/W + 2b)/s = (1/W) \sin \lambda + (2\rho a/s) = (1/W) \sin \lambda + \rho r/s = \sin \lambda (1/W + \rho \tan \beta)$ (where s , r ,
 S82 λ and β all refer now to the suture spiral, W is the whorl expansion rate [Eq.[S4] below], and
 S83 using the relations $\rho = b/a$, $r = 2a$, and $r = z \tan \beta = s \sin \lambda \tan \beta$). In any case, all these ratios
 S84 are constants for self-similar logarithmic conispiral shells.

S85 **S3 Whorl-overlap condition for non-circular and displaced generating curves**

S86 Mathematical and computational shell modeling got a boost with the work of David Raup in
 S87 the 1960s ([Raup 1961](#); [Raup & Michelson 1965](#); [Raup 1966](#)) that also kick-started theoretical
 S88 morphology. [Raup's](#) model for gastropod shell coiling ([Raup 1961, 1966](#); [Raup & Michelson](#)
 S89 [1965](#)) contains four parameters that are designed to be estimated from sagittal cross-sections
 S90 of shells. His whorl expansion rate, W , is related to γ through

$$S91 \quad W = e^{2\pi\gamma}. \quad [S4]$$

S92 His translation rate, T , is related to β by

$$S93 \quad T = \cot \beta. \quad [S5]$$

S94 The *displacement* parameter, D , measures relative distance of the aperture from the coiling
 S95 axis, and is given by

$$S96 \quad D = \frac{r - a}{r + a}, \quad [S6]$$

S97 where a is aperture radius in the r -direction (i.e., half the aperture's width in the
 S98 r -direction). The umbilicus (or columellar) radius, ξ , i.e., distance of innermost aperture
 S99 margin to the coiling axis, and the aperture size, a , are then given by

$$S100 \quad a = \left(\frac{1-D}{1+D}\right)r, \quad [S7]$$

$$S101 \quad \xi = r - a = \left(\frac{2D}{1+D}\right)r.$$

S101 Raup's fourth parameter, S , broadly defines the shape of the generating curve, and is never
 S102 really defined in Raup's formulation. In principle, it may be vector- or function-valued, e.g.,
 S103 $S = S(\varphi)$ (φ being some parameterization of the generating curve). It is, however, very often
 S104 taken to be some ratio of major and minor axes of an ellipse — a natural extension of the
 S105 circular generating curve (Raup 1966; Kohn & Riggs 1975; Newkirk & Doyle 1975; McNair
 S106 *et al.* 1981; Ekaratne & Crisp 1983; Kemp & Bertness 1984; Ackerly 1992; Stone 1995; McGhee
 S107 1999; Clarke *et al.* 1999; Urdy *et al.* 2010; Larsson *et al.* 2020). Here, I follow Ekaratne & Crisp
 S108 (1983) and define aperture size a , perpendicular to the coiling axis, and aperture size b ,
 S109 parallel to the axis, as illustrated in Fig. 1F of main text.

S110 The centers of two consecutive whorls (separated by $\Delta\theta = 2\pi$) are at distances r and rW
 S111 from the coiling axis. Their distances to the apex are $r\sqrt{1+T^2}$ and $rW\sqrt{1+T^2}$, respectively.
 S112 Aperture sizes along the conical envelope of the centerline spiral, i.e., at angle β to the coiling
 S113 axis, are given by the radii of the elliptic generating curves at that angle $\frac{\rho a}{\sqrt{\rho^2 \sin^2 \beta + \cos^2 \beta}}$ and
 S114 $\frac{\rho a W}{\sqrt{\rho^2 \sin^2 \beta + \cos^2 \beta}}$ respectively, where $\rho = b/a$. The whorl overlap condition is therefore,

$$S115 \quad r(W-1)\sqrt{1+T^2} < \frac{a\rho(W+1)\sqrt{1+T^2}}{\sqrt{\rho^2 + T^2}}. \quad [S8]$$

S116 (recall that $T = \cot \beta$, and so $\sin^2 \beta = \frac{1}{1+T^2}$ and $\cos^2 \beta = \frac{T^2}{1+T^2}$). Substituting the expression for
 S117 a from Eq.[S7], and further trivial manipulations give

$$S118 \quad T^2 < \rho^2 \left(\frac{\left(\frac{1-D}{1+D}\right)^2 (W+1)^2 - (W-1)^2}{(W-1)^2} \right), \quad [S9]$$

S119 or

$$S120 \quad T^2 < \rho^2 \frac{4W + 4D^2W - 4DW^2 - 4D}{(1 + D)^2(W - 1)^2}. \quad [S10]$$

S121 For a circular aperture ($\rho = 1$) touching the coiling axis ($D = 0$), I obtain Raup's (1966)
S122 expression for the "univalve-bivalve" boundary, $T = \frac{2\sqrt{W}}{W-1}$, on the W - T face of his
S123 morphospace cube. Substituting $T = 0$ in Eq.[S8] gives the "univalve-bivalve" boundary on
S124 the W - D face, $D < 1/W$, which is Raup's (1966) whorl-overlap condition for planispiral
S125 shells.

S126 In terms of γ and β , Eq.[S9] can be rewritten as

$$S127 \quad \cot^2 \beta < \rho^2 \left(\left(\frac{1-D}{1+D} \right)^2 \coth^2(\pi\gamma) - 1 \right) = \rho^2 \left(\left(\frac{1-D}{1+D} \right)^2 \frac{1}{\sinh^2(\pi\gamma)} - \frac{4D}{(1+D)^2} \right) \quad [S11]$$

S128 or

$$S129 \quad \tan \beta > \frac{1+D}{\rho} \frac{\sinh(\pi\gamma)}{\sqrt{(1-D)^2 - 4D \sinh^2(\pi\gamma)}}. \quad [S12]$$

S130 For circular apertures ($a = b$; $\rho = 1$) and $D = 0$, this equation gives the expression of Raup's
S131 whorl-overlap boundary in terms of γ and β of this study, $\tan \beta = \sinh(\pi\gamma)$.

S132 From Eq.[S11] one can get the condition for whorl-overlap in terms of $\sin \beta$,

$$S133 \quad \sin^2 \beta > \frac{1}{\rho^2 \left(\frac{1-D}{1+D} \right)^2 \coth^2(\pi\gamma) + (1 - \rho^2)}. \quad [S13]$$

S134 For $D = 0$ this simplifies to

$$S135 \quad \sin^2 \beta > \frac{\sinh^2(\pi\gamma)}{\sinh^2(\pi\gamma) + \rho^2}. \quad [S14]$$

S136 For $D = 0$ and $\rho = 1$, the condition further reduces to $\sin \beta > \tanh \pi\gamma$, the expression arrived
S137 at by (Clarke *et al.* 1999) (after correcting their typo and accounting for difference in
S138 definition of apical semiangle).

S139 Combining Eq.[S12] and Eq.[S2], I get the whorl-overlap boundary in terms of lead angle,

$$S140 \quad \tan \lambda < \frac{\rho}{1+D} \frac{\gamma \sqrt{(1-D)^2 - 4D \sinh^2(\pi\gamma)}}{\sqrt{1 + \gamma^2} \sinh(\pi\gamma)}. \quad [S15]$$

S141 Applying the small- γ approximation, the whorl overlap condition for lead angle becomes

$$S142 \quad \tan \lambda < \left(\frac{1-D}{1+D} \right) \frac{\rho}{\pi} + \mathcal{O}(\gamma^2), \quad [S16]$$

S143 providing the corresponding fixed value of lead angle that matches the whorl overlap
S144 condition for particular aperture shape, ρ , and aperture displacement, D .

S145 **S4 Approximation errors**

S146 For the range of γ -values exhibited by most gastropods, $\gamma \leq 0.2$ (Thompson [1942] 1992;
S147 Cameron 1981), the error between the full and approximate versions of Eq.[S2] (Eq.[2] in the
S148 main text) is no more than 2%. This is derived from the ratio of the right-hand-sides of Eq.[2]
S149 and Eq.[S2], $\sqrt{1 + \gamma^2}$, which clearly increases with γ , and is 1 for $\gamma = 0$ and 1.0198 for $\gamma = 0.2$.

S150 Similarly, for approximating radius, r , as the θ -derivative of base arc length, ℓ , using
S151 Eq.[S3], the exact expression is $d\ell/d\theta = r\sqrt{1 + \gamma_r^2}$. If γ_r is again no more than 0.2, we obtain
S152 again maximum error of 2%. This is mostly relevant for simulating logarithmic slant helices
S153 with the web application (§S6, §S7).

S154 **S5 Differential geometric parameterization**

S155 The typical approach in differential geometry is to follow the Frenet frame, attached to a
S156 space curve; though other local (moving) frames are possible (Moulton & Goriely 2012;
S157 Moulton *et al.* 2012; Uzunoğlu *et al.* 2016; Goriely 2017; Güzelkardeşler & Şahiner 2024 ; see
S158 below). The Frenet frame is composed of the tangent, principal normal, and binormal unit
S159 vectors of the space curve, $\hat{\mathbf{t}}$, $\hat{\mathbf{n}}$, and $\hat{\mathbf{b}}$, respectively, parameterized by arclength, s , along the
S160 curve. The frame changes along the curve according to the Frenet-Serret differential
S161 equations,

$$\begin{aligned}\hat{\mathbf{t}}' &= \frac{d\hat{\mathbf{t}}}{ds} = \mathbf{u} \times \hat{\mathbf{t}} = \kappa \hat{\mathbf{n}} \\ \hat{\mathbf{n}}' &= \mathbf{u} \times \hat{\mathbf{n}} = \tau \hat{\mathbf{b}} - \kappa \hat{\mathbf{t}} \\ \hat{\mathbf{b}}' &= \mathbf{u} \times \hat{\mathbf{b}} = -\tau \hat{\mathbf{n}},\end{aligned}\tag{S17}$$

S163 where \times is vector cross-product in 3D Euclidean space, \mathbf{u} is the Darboux vector,

$$\mathbf{u} = u\hat{\mathbf{u}} = \tau\hat{\mathbf{t}} + \kappa\hat{\mathbf{b}},\tag{S18}$$

S165 u is the vector's magnitude (i.e., local coiling; or the compound curvature of Nutbourne &
S166 Martin 1988; see §S1), $\kappa = u \cos \lambda$ is curvature, and $\tau = u \sin \lambda$ is torsion. The Darboux vector,
S167 thus, describes the instantaneous rotation of the Frenet moving-frame, with respect to
S168 arclength (rather than time). For generalized helices ($\tau/\kappa = \tan \lambda = \text{const}$), including conical
S169 helices, the direction of the Darboux vector is fixed, $\hat{\mathbf{u}}' = 0$, though coiling rate, u , itself can

S170 change (e.g., for conical helices $u \propto 1/s$). In other words, for generalized helices $\mathbf{u}' = u'\hat{\mathbf{u}}$, and
 S171 the direction $\hat{\mathbf{u}}$ determines the fixed coiling axis of the helix.

S172 If lead angle changes with arclength, the space curve is no longer a generalized helix, and
 S173 the direction of \mathbf{u} changes along the curve, $\hat{\mathbf{u}}' \neq 0$ and $\mathbf{u}' = u'\hat{\mathbf{u}} + u\hat{\mathbf{u}}'$. Because $\hat{\mathbf{u}}$ is a unit
 S174 vector, its derivative can be written as a cross-product with some instantaneous rotation
 S175 vector, \mathbf{w} , such that $\hat{\mathbf{u}}' = \mathbf{w} \times \hat{\mathbf{u}}$. For generalized helices $\mathbf{w} \equiv \mathbf{u}$, and so $\hat{\mathbf{u}}' = \mathbf{u} \times \hat{\mathbf{u}} = u\hat{\mathbf{u}} \times \hat{\mathbf{u}} \equiv 0$.
 S176 In the general case, we write $\mathbf{w} = w_1\hat{\mathbf{t}} + w_2\hat{\mathbf{n}} + w_3\hat{\mathbf{b}}$, and attempt to find the w_i from
 S177 Eqs.[S17] and [S18].

S178 First, note that from Eq.[S18] $\hat{\mathbf{u}} = \hat{\mathbf{t}} \sin \lambda + \hat{\mathbf{b}} \cos \lambda$, and therefore by applying the
 S179 Frenet-Serret relations (Eq.[S17]), $\hat{\mathbf{u}}' = (\hat{\mathbf{t}} \cos \lambda - \hat{\mathbf{b}} \sin \lambda)\lambda'$. Expanding the rotation vector,
 S180 $\mathbf{w} \times \hat{\mathbf{u}} = (-w_2\hat{\mathbf{b}} + w_3\hat{\mathbf{n}}) \sin \lambda + (-w_1\hat{\mathbf{n}} + w_2\hat{\mathbf{t}}) \cos \lambda$. Equating the two expressions per
 S181 component, one obtains $w_2 = \lambda'$, and $w_3 = w_1 \cot \lambda$, while w_1 still remains unknown. We can
 S182 already guess, based on $\mathbf{w} = \mathbf{u}$ for generalized helices, that $w_1 = u \sin \lambda = \tau$ and
 S183 $w_3 = u \cos \lambda = \kappa$. That is corroborated by noting that the Darboux vector does not have a
 S184 $\hat{\mathbf{n}}$ -component, i.e., $\hat{\mathbf{u}}$ and $\hat{\mathbf{n}}$ are always perpendicular to each other. Consequently, we can
 S185 construct the alternative orthonormal moving-frame of [Uzunoğlu et al. \(2016\)](#) and
 S186 [Güzelkardeşler & Şahiner \(2024\)](#), composed of $\hat{\mathbf{u}}$, $\hat{\mathbf{n}}$, and $\hat{\mathbf{u}} \times \hat{\mathbf{n}}$. The rotation vector of this
 S187 frame is \mathbf{w} , resulting in the relation $\hat{\mathbf{n}}' = \mathbf{w} \times \hat{\mathbf{n}} = w_1\hat{\mathbf{b}} - w_3\hat{\mathbf{t}}$. But from the Frenet-Serret
 S188 equations (Eq.[S17]) we know that $\hat{\mathbf{n}}' = \tau\hat{\mathbf{b}} - \kappa\hat{\mathbf{t}}$, and so $w_1 = \tau$ and $w_3 = \kappa$, or in vector form,

$$\begin{aligned}
 \mathbf{w} &= w\hat{\mathbf{w}} = \mathbf{u} + \lambda'\hat{\mathbf{n}} = u\hat{\mathbf{u}} + \lambda'\hat{\mathbf{n}}, \\
 w &= \sqrt{u^2 + (\lambda')^2},
 \end{aligned}
 \tag{S19}$$

S190 the vector and rate of global coiling, respectively. Comparing again to [Uzunoğlu et al. \(2016\)](#)
 S191 and [Güzelkardeşler & Şahiner \(2024\)](#), u is their ‘first alternative curvature’, and λ' their
 S192 ‘second alternative curvature’. Generalized helices are obtained when the second alternative
 S193 curvature vanishes, $\lambda' = 0$ ([Güzelkardeşler & Şahiner 2024](#)). Substituting the identity
 S194 $\tan \lambda = \kappa/\tau$ into their expression for the second alternative curvature, $\frac{\kappa^2}{\kappa^2 + \tau^2}(\kappa/\tau)'$, clearly
 S195 results in $\cos^2 \lambda \, d \tan \lambda / ds$, which reduces to simply $d\lambda / ds \equiv \lambda'$. Namely, the second
 S196 alternative curvature is simply the rate of change in lead angle.

S197 For generalized helices ($\lambda = \text{const}$), $\mathbf{w} = \mathbf{u}$, $\hat{\mathbf{u}}' = \mathbf{w} \times \hat{\mathbf{u}} = -\lambda'(\hat{\mathbf{u}} \times \hat{\mathbf{n}}) = 0$, and there is a fixed
S198 coiling axis, coinciding with a fixed Darboux vector. However, in general, the vector \mathbf{w}
S199 defines a precession of the Darboux vector (recall that \mathbf{u} is the instantaneous rotation of the
S200 Frenet frame), and is itself not fixed. In some special cases, when $u = \text{const}$ and \mathbf{w} fixed, one
S201 can obtain the ‘modulated curves’ of [Nutbourne & Martin \(1988\)](#), better known as ‘curves of
S202 constant precession’ ([Scofield 1995](#)).

S203 A slant helix is, similarly, a class of precession curves that includes the generalized helix
S204 and the curves of constant precession as special cases. The defining feature of a slant helix is
S205 a constant angle between the principal normal of the curve, $\hat{\mathbf{n}}$, and some fixed direction in
S206 space. In generalized helices, that angle is 90° . [Izumiya & Takeuchi’s \(2004\)](#) necessary and
S207 sufficient condition for a slant helix translates, in the notation of this study, to the
S208 proportionality relationship $\lambda' = \sigma u$. In other words, second alternative curvature is
S209 proportional to first alternative curvature, with a proportionality constant σ . The global
S210 coiling vector becomes $\mathbf{w} = u\hat{\mathbf{w}} = u(\hat{\mathbf{u}} + \sigma\hat{\mathbf{n}})$, and $\hat{\mathbf{w}}$ defines a fixed axis of rotation (or
S211 coiling), though coiling rate, $w = u\sqrt{1 + \sigma^2}$, around the fixed axis generally varies. That can
S212 be verified by $\sqrt{1 + \sigma^2}\hat{\mathbf{w}}' = (\hat{\mathbf{u}} + \sigma\hat{\mathbf{n}})' = \mathbf{w} \times \hat{\mathbf{u}} + \sigma\mathbf{w} \times \hat{\mathbf{n}} = (\sigma u\hat{\mathbf{n}}) \times \hat{\mathbf{u}} + \sigma(u\hat{\mathbf{u}} \times \hat{\mathbf{n}}) = 0$.

S213 **S6 Logarithmic slant helix**

S214 For the logarithmic slant helix, $u = \tilde{u}/s$. Consequently, $\lambda' = \sigma\tilde{u}/s$ and $w = \tilde{w}/s$, where
S215 $\tilde{w} = \tilde{u}\sqrt{1 + \sigma^2}$. Given that $d\theta/ds = w$, it is straightforward to get relations comparable to
S216 conical helices for revolution angle and arclength, $\theta = \tilde{w}\ln(s/s_0)$ and $s = s_0e^{\gamma\theta}$, where
S217 $\gamma = 1/\tilde{w}$ (in this section, $\gamma \equiv \gamma_s$). Given $\lambda' = d\lambda/ds = \sigma u = \sigma w/\sqrt{1 + \sigma^2} =$
S218 $(\sigma/\sqrt{1 + \sigma^2}) d\theta/ds$, lead angle increases linearly with revolution angle according to
S219 $\lambda = \lambda_0 + c\theta$, where $c = \sigma/\sqrt{1 + \sigma^2}$. From these expressions one can obtain (approximately) the
S220 position vector of the logarithmic slant helix, $z(\theta)$ and $r(\theta)$.

S221 Recalling that $dz/ds = \sin\lambda$ and that $d\ell/ds = \cos\lambda$, one can obtain the derivatives w.r.t
S222 to revolution angle $dz/d\theta = \sin(\lambda_0 + c\theta)s_0\gamma e^{\gamma\theta}$ and $d\ell/d\theta = \cos(\lambda_0 + c\theta)s_0\gamma e^{\gamma\theta}$. Recall
S223 from [§S2](#), that for small expansion rates $r(\theta) \approx d\ell/d\theta$, and so we obtain an approximate

S224 expression for the radius of a logarithmic slant helix,

$$S225 \quad r(\theta) \approx \gamma s_0 e^{\gamma\theta} \cos(\lambda_0 + c\theta). \quad [S20]$$

S226 Applying Eq.[S20] to the definition of the allometric exponent of r w.r.t to s , $d \ln r / d \ln s$,

S227 one obtains $d \ln r / d \ln s = \tilde{w} d \ln r / d\theta \approx \tilde{w} d (\ln \cos(\lambda(\theta)) + \gamma\theta) / d\theta = \tilde{w}(\gamma - c \tan \lambda) =$

S228 $1 - \sigma \tilde{w} \tan \lambda$.

S229 Expressions for $z(\theta)$ and $\ell(\theta)$ are obtained by integration of the aforementioned

S230 derivatives,

$$S231 \quad z(\theta) = C_z + \frac{\gamma^2 \sin(\lambda_0 + c\theta) - c\gamma \cos(\lambda_0 + c\theta)}{\gamma^2 + c^2} s_0 e^{\gamma\theta}, \quad [S21]$$

$$S232 \quad \ell(\theta) = C_\ell + \frac{\gamma^2 \cos(\lambda_0 + c\theta) + c\gamma \sin(\lambda_0 + c\theta)}{\gamma^2 + c^2} s_0 e^{\gamma\theta}, \quad [S22]$$

S234 where C_z and C_ℓ are determined from initial conditions. These expressions for $z(\theta)$, $r(\theta)$ and

S235 $\ell(\theta)$, can be used in computer graphics to simulate shells that follow a logarithmic slant helix

S236 centerline.

S237 **S7 Web application**

S238 For this study, I have also written a WebGL application to help with creating images of shells,

S239 as in Fig. 1A–C,E–I. A snapshot of the code, coinciding with the publication of this report, is

S240 available at <https://doi.org/10.5281/zenodo.19762139>.

S241 • For Fig. 1A–C the app's start values were used, with Shell deselected, Centerline spiral

S242 selected, and either Planispirals (panel A) or Circular helix (panel C) additionally

S243 selected. Pitch angle 69° , Roll angle 120° , $\lambda_0 = 0.22$, $\tilde{w} = 11.43$ ($\gamma = 0.0875$), $\sigma = 0$.

S244 • Parameters for Fig. 1E are Pitch angle 270 , Roll angle 241 , Shell and Multispirals

S245 checked. $\lambda_0 = 0.39$, $\tilde{w} = 9.38$ ($\gamma = 0.107$), $\sigma = 0$.

S246 • For Fig. 1F, Pitch angle 70 , Roll angle 53 . Shell, Centerline spiral, and Generating curve

S247 checked. $\lambda_0 = 0.22$, $\tilde{w} = 11.43$ ($\gamma = 0.0875$), $\sigma = 0$.

S248 • Parameters for Fig. 1G are Pitch angle 69 , Roll angle 120 , Shell deselected, Centerline

S249 spiral checked, $\lambda_0 = 0$, $\tilde{w} = 11.43$ ($\gamma = 0.0875$), $\sigma = 0.013$.

- S250 • For Fig. 1H, Pitch angle 64, Roll angle 0, Shell and Centerline spiral checked, $\lambda_0 = 0$,
S251 $\tilde{w} = 12.07$ ($\gamma = 0.0829$), $\sigma = 0.012$.
- S252 • For Fig. 1I, Pitch angle 55, Roll angle 239, Shell, Centerline spiral, and Generating curve
S253 checked, $\lambda_0 = 0$, $\tilde{w} = 7.29$ ($\gamma = 0.137$), $\sigma = 0.104$.

S254 S8 Supplementary references

- S255 Ackerly SC (1992). The structure of ontogenetic variation in the shell of *Pecten*.
S256 *Palaeontology* 35: 847–867.
- S257 Cameron RAD (1981). Functional aspects of shell geometry in some british land snails. *Biol J*
S258 *Linn Soc* 16: 157–167. <https://doi.org/10.1111/j.1095-8312.1981.tb01648.x>.
- S259 Chouaieb N, Goriely A, Maddocks JH (2006). Helices. *Proc Natl Acad Sci USA* 103: 9398–9403.
S260 <https://doi.org/10.1073/pnas.0508370103>.
- S261 Clarke RK, Grahame J, Mill PJ (1999). Variation and constraint in the shells of two sibling
S262 species of intertidal rough periwinkles (gastropoda: Littorina spp.). *J Zool* 247: 145–154.
S263 [10.1111/j.1469-7998.1999.tb00978.x](https://doi.org/10.1111/j.1469-7998.1999.tb00978.x).
- S264 De Renzi M, Mayoral E (2024). Understanding behaviour through theoretical morphology:
S265 the case of helical-shaped burrows. *J Iber Geol* 50: 549–566.
S266 <https://doi.org/10.1007/s41513-024-00249-7>.
- S267 Ekaratne SUK, Crisp DJ (1983). A geometric analysis of growth in gastropod shells, with
S268 particular reference to turbinate forms. *Journal of Marine Biology Association UK* 63:
S269 777–797.
- S270 Goriely A (2017). *The Mathematics and Mechanics of Biological Growth*. Springer.
S271 <https://doi.org/10.1007/978-0-387-87710-5>.
- S272 Güzelkardeşler G, Şahiner B (2024). An alternative approach to find the position vector of a
S273 general helix. *Celal Bayar University Journal of Science* 20: 54–60.
S274 [10.18466/cbayarfbe.1479066](https://doi.org/10.18466/cbayarfbe.1479066).
- S275 Hauser K, He Y, Garcia-Diaz M, Simmerling C, Coutsiyas E (2017). Characterization of

- S276 biomolecular helices and their complementarity using geometric analysis. *Journal of*
S277 *Chemical Information and Modeling* 57: 864–874.
S278 <https://doi.org/10.1021/acs.jcim.6b00721>. PMID: 28287728.
- S279 Illert C (1983). The mathematics of gnomonic seashells. *Math Biosci* 63: 21–56.
- S280 Izumiya S, Takeuchi N (2004). New special curves and developable surfaces. *Turkish Journal*
S281 *of Mathematics* 28: 153–164.
- S282 Kemp P, Bertness MD (1984). Snail shape and growth rates: evidence for plastic shell
S283 allometry in *Littorina littorea*. *Proc Natl Acad Sci USA* 81: 811–813.
S284 <https://doi.org/10.1073/pnas.81.3.811>.
- S285 Kohn AJ, Riggs AC (1975). Morphometry of the *Conus* shell. *Syst Zool* 24: 346–359.
- S286 Larsson J, Westram AM, Bengmark S, Lundh T, Butlin RK, Butlin RK (2020). A
S287 developmentally descriptive method for quantifying shape in gastropod shells. *J R Soc*
S288 *Interface* 17. <http://dx.doi.org/10.1098/rsif.2019.0721>.
- S289 Løvtrup S, von Sydow B (1974). D’arcy Thompson’s theorem and the shape of the molluscan
S290 shell. *Bull Math Biol* 36: 567–575.
- S291 McGhee GR (1999). *Theoretical Morphology: The Concept and Its Applications*. Perspectives in
S292 Earth History and Paleobiology. Columbia University Press, New York.
- S293 McNair C, Kier W, LaCroix P, Linsley R (1981). The functional significance of aperture form
S294 in gastropods. *Lethaia* 14: 63–70.
- S295 Moseley H (1842). On conchylometry. *Lond Edinb Dubl Phil Mag* 21: 300–305.
- S296 Moulton D, Goriely A, Chirat R (2012). Mechanical growth and morphogenesis of seashells. *J*
S297 *Theor Biol* 311: 69–79. <https://doi.org/10.1016/j.jtbi.2012.07.009>.
- S298 Moulton DE, Goriely A (2012). Surface growth kinematics via local curve evolution. *J of*
S299 *Math Biol* 68: 81–108.
- S300 Newkirk GF, Doyle RW (1975). Genetic analysis of shell-shape variation in *Littorina saxatilis*
S301 on an environmental cline. *Mar Biol* 30: 227–237. [10.1007/BF00390745](https://doi.org/10.1007/BF00390745).
- S302 Noshita K, Asami T, Ubukata T (2012). Functional constraints on coiling geometry and

- S303 aperture inclination in gastropods. *Paleobiology* 38: 322–334. [10.1666/10060.1](https://doi.org/10.1666/10060.1).
- S304 Nutbourne AW, Martin RR (1988). *Differential geometry applied to curve and surface design*.
S305 Ellis Horwood, Chichester, England.
- S306 O’Neill B (2006). *Elementary Differential Geometry*. Revised 2nd edn. Academic Press.
- S307 Raup DM (1961). The geometry of coiling in gastropods. *Proc Natl Acad Sci USA* 47: 602–609.
S308 <https://doi.org/10.1073/pnas.47.4.602>.
- S309 Raup DM (1966). Geometric analysis of shell coiling: general problems. *J Paleontol* 40:
S310 1178–1190.
- S311 Raup DM, Graus RR (1972). General equations for volume and surface area of a
S312 logarithmically coiled shell. *Mathematical Geology* 4: 307–316.
- S313 Raup DM, Michelson A (1965). Theoretical morphology of the coiled shell. *Science* 147:
S314 1294–1295.
- S315 Schindel DE (1990). Unoccupied morphospace and the coiled geometry of gastropods:
S316 architectural constraint or geometric covariation? In *Causes of Evolution: a paleontological*
S317 *perspective* (edited by Ross R, Allmon W), pp. 270–304. University of Chicago Press,
S318 Chicago.
- S319 Scofield PD (1995). Curves of constant precession. *The American Mathematical Monthly* 102:
S320 531–537. <https://doi.org/10.1080/00029890.1995.12004613>.
- S321 Stone JR (1995). CerioShell: a computer program designed to simulate variation in shell form.
S322 *Paleobiology* 21: 509–519.
- S323 Thompson DW ([1942] 1992). *On Growth and Form: The Complete Revised Edition*. Dover,
S324 New York.
- S325 Urdy S, Goudemand N, Bucher H, Chirat R (2010). Allometries and the morphogenesis of the
S326 molluscan shell: a quantitative and theoretical model. *J Exp Zool* 314B: 280–302.
S327 [10.1002/jez.b.21337](https://doi.org/10.1002/jez.b.21337).
- S328 Uzunoğlu B, İsmail Gök, Yaylı Y (2016). A new approach on curves of constant precession.
S329 *Applied Mathematics and Computation* 275: 317–323.

S330 <https://doi.org/10.1016/j.amc.2015.11.083>.

S331 Vermeij GJ (1993). *A Natural History of Shells*. Princeton University Press, Princeton, Oxford.